Chapter

Recent Advances in Infrared Nonlinear Optical Crystal

Senthil Kumar Chandran, Chinnakannu Elavarasi, Srinivasan Manikam and Gnanapragasam John James

Abstract

The search and growth of nonlinear optical (NLO) crystals in the infrared (IR) area are significant and of high importance in the fields of NLO, signal communication, solid-state chemistry, and laser frequency conversion. Infrared NLO crystals have a wide IR transparent range, high laser damage threshold (LDT) value, and large NLO coefficients. This chapter presents the recent advances in IR-NLO crystals and especially emphasizes their crystal growth method, crystal structures, band gap value, LDT, and NLO properties. Based on its structural variety, it is categorized into chalcogenides, chalcohalides, oxides, halides, and oxyhalides. This chapter describes several kinds of IR-NLO crystals and their structural, band gap value, thermal, optical, LDT, and NLO properties and also describes the significance of these crystals in laser frequency conversion, optical parameter oscillator, and other optical applications.

Keywords: crystal growth, laser-induced damage thresholds, infrared crystal, transmittance, optical parameter oscillator

1. Introduction

Nonlinear optical (NLO) crystals are important for frequency conversion and are widely used in different laser-oriented applications. High-efficiency NLO crystals need in high-efficiency laser methods, so it is essential to growing novel NLO crystals with good properties. In the past five decades, many valuable NLO crystals in the near-infrared (NIR), visible, and ultraviolet areas have been commercialized, such as $LiNbO_3$, LiB_3O_5 (LBO), β-BaB_2O_4 (β-BBO), $KTiOPO_4$ (KTP), and KH_2PO_4 (KDP). These crystals are commonly used in basic science and technology, such as laser generation, artificial nuclear fusion, and so on. However, due to the increasing practical or market necessities, only a few crystals can be successfully used in deep-UV(DUV) and mid/far-IR areas. Nevertheless, NLO crystals that can powerfully produce high-power mid-IR lasers in the spectral area of 2–25 μm are very rare. Up to now, several useful NLO crystals have been originated and used in DUV, UV-Vis, and near IR, but they cannot be implemented in mid-infrared spectra because they have two atmospheric transparent regions, 3–5 and 8–14 mm, owing to strong absorption [1–5].

Second-order nonlinear optical (NLO) crystals are significant for producing coherent energy in the IR region (3–20 μm). IR lasers have several vital applications in various devices, such as optical parametric oscillators (OPO), remote sensing, optical sensing, instrumental spectroscopy, industry, military, analytical devices optical imaging, laser guidance, telecommunication, medical diagnostics, and long-distance communications. Such instruments are used to identify various elements and precise vibrational spectra [6–9]. Even after several years of deep research, only three unresolved NLO crystals have been commercially accessible in the mid and far-IR areas, namely, $AgGaSe_2$, $AgGaS_2$, and $ZnGeP_2$. However, some inadequacies still exist in these IR-NLO crystals, such as the inherent efficiency loss arising from dual photon absorption, low MIR cut-off edge, non-phase matchable behavior, and low laser damage threshold. Already commercial ones cannot meet the commercial conditions because of their inherent disadvantages. Hence, it is essential to find out new efficient MIR NLO crystals with more stable efficiency [3, 7, 8, 10].

The large size high-quality mid-IR-NLO crystals for laser device applications are grown by Bridgman-Stockbarger (BS) method and molecular beam epitaxy (MBE) growth method [5]. The IR-NLO crystal can be separated into five categories: chalcogenides, chalcohalides, oxides, oxyhalides, halides, and chalcohalides [4]. This chapter will emphasize second-order NLO inorganic crystals in the MIR region. We did not focus on the commercially accessible $LiNbO_3$, LiB_3O_5 (LBO), β-BaB_2O_4 (β-BBO), KH_2PO_4, and $KTiOPO_4$ NLO crystals, these crystals have absorption bands in this region. Instead, this chapter focus on the chalcogenides, chalcohalides, oxides, halides, and oxyhalides. These crystals are promising materials for MIR applications due to they have wide transmittance in the MIR region [11].

2. Main conditions at NLO crystal select for changing coherent energy in the IR region

The selection of high-quality crystals is mainly tough when designing new, appropriate NLO crystals for the IR region. It should be highlighted that the balance between SHG coefficients and energy gap is an important feature to attain noble optical functioning in a mid-IR-NLO crystal [3]. The mid-IR-NLO crystals are significant to develop high-power tunable laser output extending the two atmospheric bands (3–5 μm and 8–14 μm) [4]. The accessibility of bulk-size single crystals is vital for the production of NLO devices. It is a great task to grow novel mid-IR-NLO crystals with desirable properties for useful applications. The good mid-IR-NLO crystals should satisfy the following basic criteria [2, 3, 6, 10, 12, 13]:

1. High second harmonic generation (SHG) responses
2. High laser damage threshold
3. Wide IR optical transparency range
4. Moderate birefringence
5. Good thermal stability
6. Good mechanical properties

7. Good facile growth of big size crystals

8. Splendid chemical stability

9. Crystal with non-centrosymmetric space group

10. Congruent-melting performance to enable single-crystal growth

11. Low absorption loss at suitable laser wavelengths

3. Chalcogenides

Chalcogenides are new kind of material denoting the chalcogen elements (sulfide, selenide, and telluride) of the group VIA. The chalcogenides are designed by covalent bonding and originate in a variety of structures, mostly formatted in octahedral or trigonal geometry. Chalcogenides are useful in many fields, such as photocatalyst, thermoelectric, MIR-NLO, photovoltaic, sensor, fuel cell, and battery [6, 14, 15]. Chalcogenides are suitable crystals for MIR-NLO as they exhibit wide transparency in IR regions and can obtain large SHG responses in this region [16]. Normally, chalcogenides are capable materials for MIR-NLO devices owing to their many benefits, such as large optical nonlinearity, broad transparency range, and large birefringence. II-IV-V_2 and I-III-VI_2 chalcopyrites are now the leading functional MIR-NLO crystals in the market and laboratory. In the past two decades, more consideration has been given to discovering chalcogenides as MIR-NLO crystals for their structural diversity. Quaternary chalcogenide crystals own a high bandgap (Eg) and high LDT. But the small nonlinearity coefficients slowed down their use in high-power laser generation. Though such kinds of crystals have many MIR-NLO benefits, many of them also have some inadequacies. To meet the requirement of laser device manufacture, some advanced growth methods are adopted to produce high purity and high-quality big size crystals of the chalcogenide. But, quaternary chalcogenide crystals, such as $Li_2Ga_2GeS_6$, LiGaGe2Se_6, $AgGaGeS_4$, and Ba_2GaGeS_6, are grown in bulk-sized crystals, which is desirable for optical devices [5, 6, 10, 16]. There are different kinds of chalcogenides, generally, alkali metal chalcogenides and transition metal chalcogenides (TMCs), which again can be categorized into binary, ternary, and quaternary chalcogenides. The chalcogenides have weaker interatomic bonds than the oxides, resulting in good optical transparencies in the IR regions. Meanwhile, the chalcogenides exhibit adjustable structure and optical properties [6, 14, 15, 17].

3.1 Cataloguing of chalcogenides based on number of components

Chalcogenides are classified based on their number of components, such as binary, ternary and quaternary structures, number of metals, number of chalcogen ions, and so on though, both ternary and quaternary elements of chalcogenides are systematically analyzed compared to binary chalcogenides [18, 19].

3.1.1 Binary chalcogenides

Binary chalcogenides containes two kinds of ions (metal ions and chalcogen anion). The CdS, CdSe, Ga_2S_3, GaS, In_2S_3, GaSe MnS, SnS, SnS_2, ZnS, and ZnSe are

an example of binary chalcogenides. For instance, CdS is one of the most considered chalcogenides. It has an energy gap value of 2.3 eV and is comparatively active under visible light. Its special size and structure-based optical and electronic properties are desirable for various kinds of applications. Owing to its numerous possible applications CDS chalcogenides are assumed to be the most significant materials [18, 19].

3.1.2 Ternary chalcogenides

When selecting a crystal for laser energy conversion in the IR, it is essential to have an ideal mixture of various considerations like birefringence value not less than 0.03 and LDT value of around 100 Mcm^{-2}, energy gap value of more than 3.3 eV and the NLO coefficient should be more than 4 pm V^{-1} [20]. The Li- and Ba-having chalcogenides meet these desires. The $ZnGeP_2$, $AgGaSe_2$, $CdSiP_2$, and $AgGaTe_2$ crystals have high NLO susceptibility, but their forbidden energy band is too low. The most commonly used nonlinear crystals for the MIR are $AgGaS_2$ $AgGaSe_2$, and $ZnGeP_2$. However, they all own serious disadvantages [6, 21, 22]. In recent times, consideration was given to chalcogenide crystals, such as alkali and alkali-earth metals (Li and Ba) (**Table 1**). These crystals permit one to resolve some difficulties in the MIR region. The birefringence value in Li-comprising crystals is significantly larger. $LiBC_2$ (B = Ga; C = S,Se) crystals can be applied for SHG applications wavelengths between 1.4 and 12 μm [23, 24]. Telluride crystals also have MIR properties, especially $LiGaTe_2$ has phase-matching in the entire transparency region. The SHG conversion efficiency of $LiGaTe_2$ is 10.6 μm, which is higher than that of AGSe [25]. To enhance the energy gap, Ag cation is to be substituted with alkali/alkaline earth metal (Li, Ba). Adding

Crystal	Point group	Transparency range (μm)	Band gap (ev)	Nonlinear coeff. (pm $V^{-}1$)	Laser damage threshold (MW $cm^{-}2$)
$AgGaS_2$	42 m	0.47–13	2.7	d32 = 8, 1.06 d36 = 19, 1.06	34 at 10 ns, 1064 nm
$ZnGeP_2$	42 m	0.74–12	2	d36=75, 9.6	100 at 10 ns, 2000 nm
$AgGaSe_2$	42 m	0.76–18	1.8	d32 = 19.6,3.4 d36 = 39, 1.06	13 at 30 ns, 2000 nm
$LiGaTe_2$	42 m	0.52–20	2.31	d36 = 43, 4.5	—
$LiGaS_2$	mm2	0.32–12	4.15	d31 = 5.8, 2.3 d24 = 5.1, 2.3	240 at 14 ns, 1064 nm
$LiGaSe_2$	mm2	0.37–14	3.57	d31 = 9.9,2.3 d24 = 7.7, 2.3	80 at 5.6 ns, 1064 nm
$LiInS_2$	mm2	0.34–13.2	3.57	d31 = 7.25 d24 = 5.66, 2.3	40* 14 ns, 1064 nm
$LiInSe_2$	mm2	0.46–14	2.86	d31 = 11.78 d24 = 8.17, 2.3	40* 10 ns, 1064 nm
$BaGa_4S_7$	mm2	0.35–13.7	3.54	d32 = 5.7, 2.3	250 at 14 ns, 1064 nm
$BaGa_4Se_7$	m	0.47–18	2.64	d11 = 18.2, 2.3 d13 = −0.6, 2.3	—

Table 1.
Point group, transparency range, band gap, and LDT value of ternary chalcogenides.

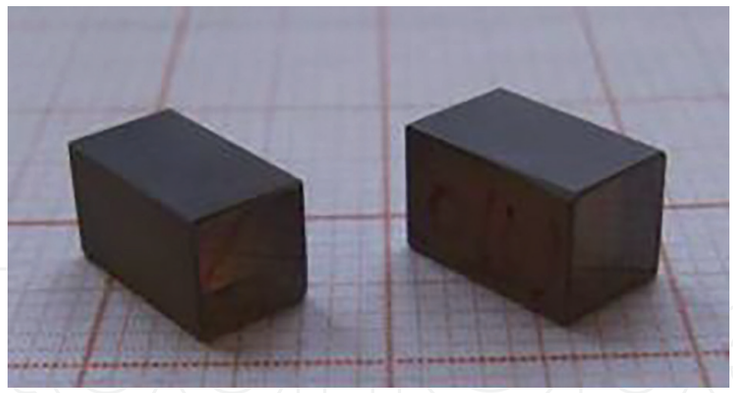

Figure 1.
Single crystals of $BaGa_4S_7$.

these metal, we can get $LiBC_2$ (B = In, Ga; C = S, Se, Te) and BaGa4C7 (C = S, Se) group crystals. These crystals own a high bandgap value [26–28]. A little mass of Li is the reason for high thermal conductivity and high vibrational frequencies. The thermal conductivity of Li mixtures is around five times higher than that of AGS (Se) [29] and four to eight times more than that of $BaGa_4S_7$ (Se) (**Figure 1**) [6, 28]. The laser damage threshold for LGS is 3.5 Jcm^{-2}, which is five times larger than LISe [30]. A similar result has been obtained when the Ag ion is substituted with Ba. $BaGa_4S_7$ crystal has high LDT and NLO susceptibility. Though, Ba cation slightly drops the band gap value. The point group is mm_2 and m for $BaGa_4S_7$ (**Figure 1**) and $BaGa_4Se_7$, respectively. Wide transparency regions of 0.35–12 and 0.47–15.0 μm, and energy gaps of 3.54 and 2.64 eV were found for both $BaGa_4S_7$ and $BaGa_4Se_7$ crystals, respectively. Both crystals have strong absorption peak at 15 μm. The $BaGa_4Se_7$ showed high nonlinear susceptibility of d_{11} = 18.2 pm V^{-1} [6, 31, 32].

3.1.3 Quaternary chalcogenides

Quaternary chalcogenides have four kinds of ions together with a chalcogen anion. These kinds of materials have different applications, such as MIR-NLO, solar cell absorbers, photocatalysts, and so on. Quaternary materials adopt different kinds of elements, which permits comparatively complex structural, electronic, and optical properties [6, 33]. Using the quaternary crystals, the IR-NLO parameters can be enhanced with a high content of NLO-active parts [6]. A compact organization of the microscopic NLO-active parts increases high macroscopic NLO outcomes [6]. The birefringence value of $AgGaSe_2$ is 0.05 and this value for $AgGaGe_3Se_8$ is 0.11. The enhanced LDT value of $AgGaGeS_4$ shows that it is a potential alternative crystal to the generally used $AgGaS_2$ for IR-NLO applications. $Li_2In_2SiSe_6$, $Li_2In_2GeSe_6$, $Li_2Ga_2GeS_6$, and $LiGaGe_2Se_6$ are the Li-having quaternary chalcogenides crystals (**Table 2**) [6, 34–37]. All these crystals have non-centrosymmetric crystal structures. $Li_2Ga_2GeS_6$ (**Figure** 2), $LiGaGe_2Se_6$ (**Figure 3**) crystals have orthorhombic crystal systems with space group Fdd_2 and $Li_2In_2GeSe_6$, Li_2In_2SiSe6 crystals own monoclinic crystal systems with space group Cc. Ba-having quaternary $BaGa_2GeS_6$, $BaGa_2GeSe_6$ structures, which are promising crystals for NLO applications [37]. The NLO susceptibilities of $Li_2Ga_2GeS_6$ are 16 pm/V, which is significantly higher than $LiGaS_2$ (5.8 pm/V). A similar result was noted for $LiGaGe_2Se_6$. $BaGa_2GeS_6$ and $BaGa_2GeSe_6$ crystals also have improved NLO parameters. The SHG experiments showed that both materials have phase-matched behavior. The calculated SHG coefficient is ~2.1 and ~3.5 times

Crystal	Point group	Transparency range (μm)	Band gap (ev)	Nonlinear coeff., (pm V^{-1})	Optical damage threshold (MW cm^{-2})
$AgGaGeS_4$	mm2	0.42–12	2.8	d31 = 15, 1.06	50 at 15 ns, 1064 nm
$AgGaGe_3Se_8$	mm2	0.6–18	2.4	d31 = 33.4	–
$Li_2Ga_2GeS_6$	mm2	0.35–14	2.51	deff = 16, 1.06	>50 at 15 ns, 1064 nm
$LiGaGe_2Se_6$	mm2	0.47–18	2.64	d15 = 18.6, 2.09	50 at 10 ns, 1064 nm
$Li_2In_2GeS_6$	m	0.36	3.45	≈d36 = 12.6, 10.6	–
$Li_2In_2GeSe_6$	m	0.54	2.30	≈d36 AGSe	–
$Li_2In_2SiS_6$	m	0.34	3.61	≈d36 AGS	–
$BaGa_2GeS_6$	3	0.38–14	3.26	deff = 26.3, 2.09	–
$BaGa_2GeSe_6$	3	0.44–18	2.81	deff = 43.7, 2.09	–

Table 2.
Point group, transparency range, band gap, and LDT value of quaternary chalcogenides.

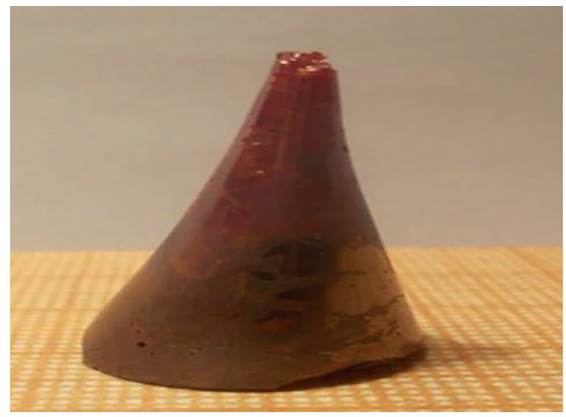

Figure 2.
Crystal of $LiGaGe_2Se_6$.

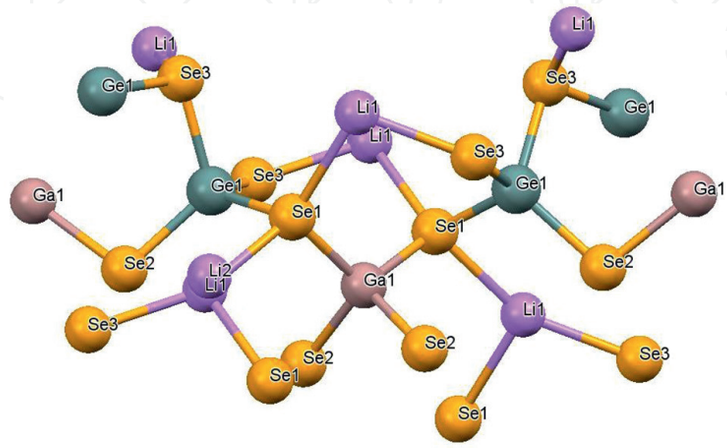

Figure 3.
Crystal structure of $LiGaGe_2Se_6$.

higher than that of $AgGaS_2$. The nonlinear susceptibilities are 26.3 pm/V and 43.7 pm/V for $BaGa_2GeS_6$ and $BaGa_2GeSe_6$, respectively [37]. The transparency region in $Li_2Ga_2GeS_6$ and $LiGaGe_2Se_6$ is 0.35–12 and 0.37–14 μm, respectively. For $BaGa_2GeS_6$ and $BaGa_2GeSe_6$, the transparency regions are 0.380–13.7 μm and 0.44–18 μm, respectively. Band gaps of $BaGa_2GeS_6$ and $BaGa_2GeSe_6$ are 3.26 and 2.81 eV, respectively. $Li_2In_2GeSe_6$ and $Li_2In_2SiSe_6$ crystals have the energy gap values of 2.30 and 3.61 eV, respectively [6].

4. Chalcohalides

Chalcohalides could be considered potential materials for mid-IR applications. The chalcohalides contain a combination of sulfur and halogen. Chalcohalides have non-centrosymmetric coordinated surroundings that can stimulate mid-IR-NLO efficiency. Based on the chemical compounds present in the chalcohalides, it can be divided into [4]:

1. Alkali/alkaline-earth metal chalcohalides

2. Adduct-type chalcohalides

3. Lewis acid adducts chalcohalides

4. Main group element clusters chalcohalides

5. Other group main metal chalcohalides

6. Transition metal chalcohalides

4.1 Alkali/alkaline-earth metal chalcohalides

The $Ba_4Ge_3S_9Cl_2$ chalcohalide has excellent mid-IR-NLO properties [38]. It has a space group $P6_3$. The bandgap energy of $Ba_4Ge_3S_9Cl_2$ was 2.91 eV. The SHG response of $Ba_4Ge_3S_9Cl_2$ was 2.4 times higher than that of AGS [38]. The bandgap of $Ba_4Ge_3S_9Cl_2$ is 2.67 eV, which was calculated by the DFT method. NLO coefficients are found to be $d_{15} = d_{24} = 7.61$ and $d_{33} = 13.81$ pm/V. The bandgap of $NaBa_4Ge_3S_{10}Cl$ was 3.49 eV and SHG efficiency was 0.3 times that of $AgGaS_2$ (AGS) [39]. The theoretically calculated bandgap of this crystal is 2.94 eV. Then, the NLO coefficients are calculated to be $d_{15} = d_{24} = 3.89$ and $d_{33} = 9.32$ pm/V. The mid-IR-NLO crystals $[A_3X]$ $[Ga_3PS_8]$ (A = K, Rb; X = Cl, Br) were synthesized and reported by B.W. Liu et al. in the year 2016 [40]. Two Cl-crystals $[K_3Cl][Ga_3PS_8]$ and $[Rb_3Cl][Ga_3PS_8]$ are having isostructural with space group Pmn_{21}, while the other two Br-crystals $[Rb_3Br][Ga_3PS_8]$ and $[K_3Br][Ga_3PS_8]$ belong to Pm space group. These four compounds showed outstanding mid-IR-NLO behavior and the energy gaps of $[K_3Cl][Ga_3PS_8]$, $[Rb_3Cl][Ga_3PS_8]$, $[K_3Br][Ga_3PS_8]$, and $[Rb_3Br][Ga_3\text{-}PS_8]$ are 3.60, 3.65, 3.85, and 3.50 eV, respectively. All four compounds showed large SHG responses of 4.0, 5.0, 7.0, and 9.0 times that of $AgGaS_2$ (AGS) at 1064 nm [39]. Moreover, these four compounds have higher laser threshold damage (LDT) of 37, 35, 31, and 29 times than that of AGS (**Table 3**).

Crystal	Space group	Band gap (ev) (DFT)	SHG $AgGaS_2$ (AGS) times	Nonlinear coefficients (pm/V)	Laser threshold damage (LDT) $AgGaS_2$ (AGS)
$Ba_4Ge_3S_9Cl_2$	$P6_3$	2.67	2.4	$d_{15} = d_{24} = 7.61$ and $d_{33} = 13.81$	–
$NaBa_4Ge_3S_{10}Cl$	—	3.49	0.3	are $d_{15} = d_{24} = 3.89$ and $d_{33} = 9.32$	–
$[K_3Cl][Ga_3PS_8]$	Pmn21	3.60	4.0	–	37
$[Rb_3Cl][Ga_3PS_8]$	Pmn21	3.65	5.0	–	35
$[K_3Br][Ga_3PS_8]$	Pm	3.85,	7.0	–	35
$[Rb_3Br][Ga_3PS_8]$	Pm	3.50	9.0	–	29

Table 3.
Space group, band gap, and LDT value of alkali/alkaline-earth metal chalcohalides.

Crystal	Space group	Band gap (ev)	SHG $AgGaS_2$(AGS) times	IR transparent ranges (μm)	NLO coefficients (pm/V)
(SbI_3) $(S8)_3$	R_3m	2.52	1.0	2.5–25.0	$d_{15} = 9.21$, $d_{22} = 9.22$, $d_{33} = 6.91$
$(AsI_3).(S_8)_3$	R_3m	2.31 eV	0.8	0.4–25.0	$d_{15} = 3.40$, $d_{22} = 6.21$, $d_{33} = 0.73$
$(SnI_4).(S_8)_2$	Fdd_2	2.17 eV	0.5	2.5–25.0	–

Table 4.
Space group, band gap, SHG, and transparency range value of adduct-type chalcohalides.

4.2 Adduct-type chalcohalides

The (SbI_3) $(S8)_3$ and (SnI_4)-$(S8)_2$ are the adduct-type of chalcohalides. The $(TI_3).(S_8)_3$ (T = As, Sb) [4, 41–44] adduct-type chalcohalides have isostructural with R_3m space group (**Table 4**). The $(SbI_3).(S_8)_3$ and $(AsI_3).(S_8)_3$ chalcohalides have reasonable energy gap value of 2.52 and 2.31 eV and their theoretical energy gaps are 2.69 and 2.21 eV, respectively. SHG responses of these two chalcohalides have 1.0 and 0.8 times that of $AgGaS_2$. They also have wide IR transparent wavelengths around 2.5–25.0 μm and 0.4–25.0 μm [41, 42]. The calculated NLO coefficients are $d_{15} = 9.21$, $d_{22} = 9.22$, $d_{33} = 6.91$ pm/V for $(SbI_3).(S_8)_3$ and $d_{15} = 3.40$, $d_{22} = 6.21$, $d_{33} = 0.73$ pm/V for $(AsI_3).(S_8)_3$. The chalcohalides $(SnI_4).(S_8)_2$ has space group Fdd_2 [44] and a wide IR window in the range of 2.5–25.0 μm. The energy gap of $(SnI_4).(S_8)_2$ is 2.17 eV. The SHG response of $(SnI_4).(S_8)_2$ is 0.5 times stronger than that of $AgGaS_2$ at 2.1 μm.

4.3 Lewis acid adduct chalcohalides

Lewis acid adduct chalcohalides have sulfur-nitrogen rings with a variety of structures. These chalcohalides have moderate band gaps and IR-NLO properties (**Table 5**). A new chalcohalide $(NSF)_4$ [45] has a space group of P-421c. The calculated energy gaps are 4.57 eV (HSE06 method) and 3.58 eV (GGA method). For a high LDT, the large bandgap is more advantageous. The birefringence for $(NSF)_4$ is 0.220 at 1064 nm and the calculated NLO coefficient for $(NSF)_4$ is $d_{14} = 3.20$ pm/V.

Crystal	Space group	Band gap (HSE06) (ev)	NLO coefficient (pm/V)
$(NSF)_4$	P-421c	4.57	d_{14} = 3.20
$S_3N_5PF_2$	R_3m	3.49	d_{15} = 1.71, d_{21} = 0.19 and d_{33} = 3.69

Table 5.
Space group and band gap, and value of Lewis acid adduct chalcohalides.

Increased bandgap occurs due to the large electronegativity of F atoms in the compound. $S_3N_5PF_2$ crystal [46] has an R_3m space group. It has a wide bandgap of 3.49 eV (HSE06). The estimated birefringence is around 0.110 at 1064 nm and NLO coefficients are d_{15} = 1.71, d_{21} = 0.19 and d_{33} = 3.69 pm/V. The d_{33} coefficient is around 9.2 times stronger than that of KDP.

4.4 Main group element clusters chalcohalides

The chalcohalides $(Bi_4S_4)(AlCl_4)_4$ belong to the space group I-4 (**Figure 4**) [47] and it has two classes of main group component clusters that are in $AlCl_4$ tetrahedron and Bi_4S_4 cube. The energy gap of $(Bi_4S_4)(AlCl_4)_4$ is calculated to be 3.59 eV. $(Bi_4S_4)(AlCl_4)_4$ is the largest main group element cluster chalcohalide, which has an NLO coefficient value of d_{14} = 1.52 pm/V and it is 3.8 times stronger than that of KDP. The DFT method showed that the main group component cluster chalcohalides has insignificant NLO coefficients.

4.5 Other main groups of metal chalcohalides

Both In_5S_5Cl [48] and In_5S_5Br [49] have isostructural properties, which are having the space groups Pmn21. The In_5S_5Cl and In_5S_5Br materials have band gap of 1.76 and 1.84 eV, respectively (**Table 6**). The estimated NLO coefficients are found to be d_{15} = 0.36, d_{24} = 2.83, d_{33} = 13.38 pm/V for In_5S_5Cl and d_{15} = 2.07, d_{24} = 2.21, d_{33} = 7.38 pm/V for In_5S_5Br. When compared with the NLO coefficients of AGS, the main group metal chalcohalides In_5S_5Cl and In_5S_5Br have d_{33}=1.0 and 0.5 times than that of AGS. The $(CS_3N_2Br)Br_3$ main group metal chalcohalides [50] crystallizes in space group Pna_{21}. The estimated energy gap for $(CS_3N_2Br)Br_3$ is 2.21 eV ($HSE0_6$), and the NLO coefficients of $(CS_3N_2Br)Br_3$ are d_{15} = 8.90, d_{24} = 5.40, d_{33} = 1.00 pm/V. From the NLO coefficient result, d_{15} has a good NLO coefficient, which is about 0.6 times that of AGS.

4.6 Transition metal chalcohalides

Asymmetric distribution of electron clouds is generally caused by polyhedron with the d_{10} transition metals because of the dp orbital hybridization and group distortion, so it produces high SHG behavior. Due to the dp hybridization, the compound has a red-shifted absorption edge, this might reduce the bandgap of IR-NLO materials. To enhance the chalcogenides energy gap, halogen elements are introduced, that is, by combining cations with d10 configuration, which led to the equilibrium among energy gaps and SHG behavior in the IR-NLO crystals. So, they separated the asymmetric chalcohalides with a d_{10} electronic configuration. The transition metal chalcohalide Ag_2HgSI_2 has the space group Cmc_{21} [51]. The bandgap of Ag_2HgSI_2 is 2.65 eV and it is compared with AGS of (2.70 eV). The SHG of Ag_2HgSI_2 is 4.2 times stronger than that of KDP. The theoretical birefringence of Ag_2HgSI_2 is 0.210 at 1064 nm. The crystal $(P4S_3)_3(CuCl)_7$ belongs to the space group $P_{31}c$ [52]. The bandgap of

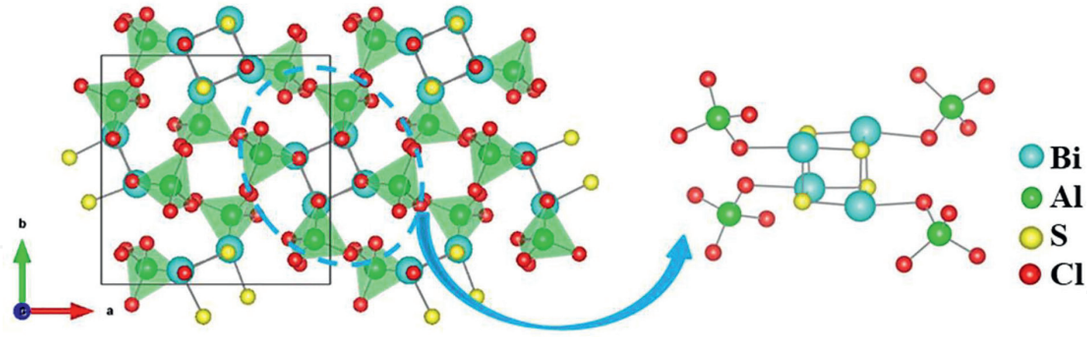

Figure 4.
Crystal structure of $(Bi_4S_4)(AlCl_4)_4$.

Crystal	Space group	Band gap (HSE06) ev	NLO coefficient (pm/V)	NLO coefficient (AGS) times
In_5S_5Cl	Pmn21	1.76	d_{15} = 0.36, d_{24} = 2.83, d_{33} = 13.38	1.0
In_5S_5Br	Pmn21	1.84	d_{15} = 2.07, d_{24} = 2.21, d_{33} = 7.38	0.5
$(CS_3N_2Br)Br_3$	Pna_{21}	2.21	d_{15} = 8.90, d_{24} = 5.40, d_{33} = 1.00	0.6

Table 6.
Space group, band gap, and SHG value of other main groups of metal chalcohalides.

$(P_4S_3)_3(CuCl)_7$ is 2.77 eV ($HSE0_6$ method) and NLO coefficients of $(P_4S_3)_3(CuCl)_7$ are d_{33} = 3.34 and d_{15} = d_{24} = 1.81 pm/V. In the NLO coefficients, the d_{33} value is about 8.5 times that of KDP and has a birefringence value of 0.150 at 1064 nm.

5. Oxide crystal

Normally, oxide-based materials have a high laser damage threshold and many of them have limited IR transparency within the range of 6 μm. Here, we would like to explain the new oxide-based NLO materials, which are very important for the development of IR transparent regions beyond 6 μm. Several new NLO oxide crystals were identified, which have high IR cutoff wavelengths that are up to 6 μm. For instance β-$BaTeMo_2O_9$ [53], $MnTeMoO_6$[54], $Cs_2TeW_3O_{12}$ [55], $V_2Te_2O_9$ [56], Li_3VO_4 [57] , M_2LiVO_4 (M = Rb, Cs) [58], $Li_2K_4TiOGe_4O_{12}$[59], and $Rb_4Li_2TiOGe_4O_{12}$[60]. Moreover, for the oxide-based NLO material, IR transparent range is a difficult factor to attain. $Pb_{17}O_8Cl_{18}$ was new IR-NLO material discovered by Pan and Poeppelmeier et al., [61] in 2015. $Pb_{17}O_8Cl_{18}$ single crystal was synthesized by modified spontaneous crystallization in an open model. Tao's et al. [62] reported a new $LiNbO_3$-type NLO crystal. Li_2ZrTeO_6 crystal (size: 16 × 15 × 12 mm^3) is grown by top-seeded solution growth (TSSG) method. To maintain the structural qualities of $LiNbO_3$, $Zr^{4+}$and Te^{6+} were substituted for Nb^{5+} to form Li_2ZrTeO_6 and it crystallized in the trigonal crystal system with space group *R*3 (**Figure 5**). $LiNbO_3$ belongs to the space group, R_3c, which has a close structural feature with Li_2ZrTeO_6 [63]. $La_3SnGa_5O_{14}$ is a new IR-NLO crystal, it belongs to the langasite family and has a space group *P*321 [64]. Polycrystalline

$La_3SnGa_5O_{14}$ was produced using a solid-state reaction and a single crystal were grown by Czochralski method. The single crystal of $Pb_{17}O_8Cl_{18}$ has a bandgap of 3.44 eV and it has high IR transparency (13.9 μm). $La_3SnGa_5O_{14}$ has a wide energy gap value of 4.60 eV and transparency of 10 μm.

The SHG responses of $Pb_{17}O_8Cl_{18}$ showed a response at 2090 nm and 1064 nm, which is phase-matchable, and it is two times stronger than that of $AgGaS_2$ and four times higher than that of KDP. Li_2ZrTeO_6 showed a huge powder SHG behavior at 1064 nm, which is 2.5 times higher than that of KDP [63]. For Li_2ZrTeO_6 and $LiNbO_3$, there is a variation in the SHG responses, which is closely correlated, and it is due to the different sizes of octahedral distortions in their crystal structure. The SHG efficiency of $La_3SnGa_5O_{14}$ is 0.4 times that of $AgGaS_2$ and when compared to $AgGaS_2$ (13 μm) it has wide IR transparency. $Pb_{17}O_8Cl_{18}$ has an LDT of 12.8 MW/cm^2 (**Table 7**). These characteristics reveal that $Pb_{17}O_8Cl_{18}$ is one of the good mid-IR-NLO crystals for the next generation. Li_2ZrTeO_6 has an outstanding optical performance and a very high LDT greater than 1.3 GW/cm^2 and it was more than 22 times that of $LiNbO_3$. It has a higher IR transparent range that is up to 7.4 μm. $La_3SnGa_5O_{14}$,which has the highest LDT of 846 MW/cm^2, is an alternative NLO crystal in the mid-IR region. It is transparent beyond 10 μm. The langasite family provided valuable information to design a new NLO crystal in the IR area.

6. Halides

A halide has a binary form in which one region is a halogen and the other region is a component or radical that is less electronegative/electropositive than the halogen [65]. For preparing NLO halides, the physical, chemical, and crystallographic aspects are important. In halides, hyperpolarizabilities were used to find out the NLO susceptibilities. Moreover, these crystals have high LDT and good mechanical properties. $HgBr_2$ crystal was grown using a lowering temperature technique with a size of about 15 × 15 × 1.5 mm^3 [66]. Tl_3PbBr_5, Tl_4PbI_6, Tl_4HgI_6, and Tl_3PbI_5 were grown by the vertical Bridgman method [5]. The 3:1:5 ratio showed orthorhombic symmetry and the 4:1:6 ratio indicated tetragonal symmetry. In this method, they maintained the temperature gradients in the range from 20 K/cm to 30 K/cm and cooling rates were in the range from 5 to 10 K/h, which showed a growth of 1 cm/day and 3–5 cm/day. Tl_3PbCl_5 [67] and Tl_3PbBr_5 [68] single crystals were grown by Bridgman-Stockbarger technique. Tl_3PbI_5 is colorless and Tl_3PbBr_5 (**Figure 6**) crystal is a yellow color and transparent. Tl_4HgI_6 crystal is grown using Bridgman-Stockbarger method [69, 70] and they melt consistently at 396°C. The crystal was red and when the iodine concentration increases in the stoichiometric ratio, the crystal becomes changed to black. It belongs to the point symmetry group C_4v. $BaMgF_4$ crystal was grown using the Czochralski technique [71]. It belongs to the pyroelectric fluoride group $BaMF_4$ (M = Mg, Co, Ni, Zn) and it has space group Cmc_{21}. $SrAlF_5$ crystal belongs to the class of uniaxial ferroelectric [72] and is grown using Czochralski technique [71]. Tl_3PbCl_5 and Tl_3PbBr_5 are nonhygroscopic. In Tl_3PbBr_5, the phase transition is observed at ~237°C, and for Tl_3PbCl_5, phase transition is noted at 171°C. Tl_2HgI_4 compound has a melting point temperature of 318°C.

$HgBr_2$ crystal showed good phase matchable SHG efficiency, which is 10 times greater than that of KDP and has transparency between 2.5 and 25 mm. It covers the whole mid-IR range. Tl_3PbCl_5 and Tl_3PbBr_5 have transparency of 0.5–20 mm and 0.65–24 mm, respectively. The Tl_4HgI_6 crystal is optically positive and transparent

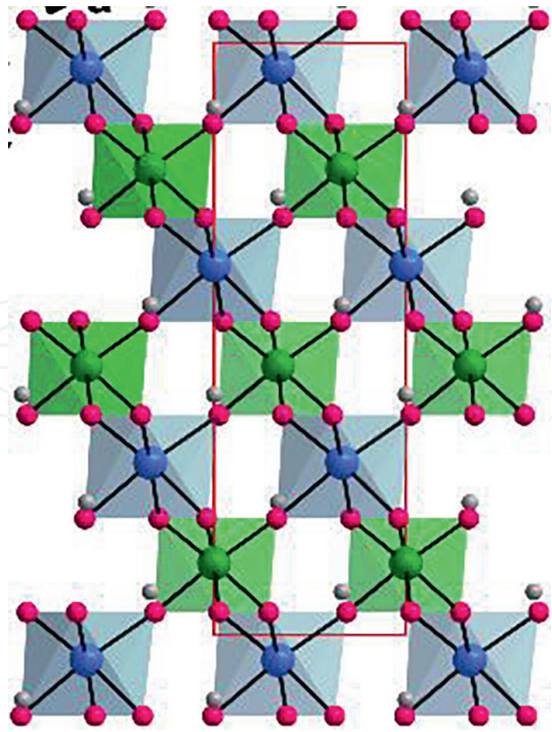

Figure 5.
Crystal structures of Li_2ZrTeO_6.

Crystal	Space group	Bandgap (eV)	IR range	SHG	LDT (× AGS, MW/cm2)
Li_2ZrTeO_6	*R*3	4.06	7.4 μm	2.5 times (KDP)	> 1300 MW/cm^2
$La_3SnGa_5O_{14}$	*P*321	4.60 eV	10 μm	0.4 times that of $AgGaS_2$	28 × AGS, 846 MW/cm2
$Pb_{17}O_8Cl_{18}$	Fmm2	3.44 eV	13.9 μm	2 times ($AgGaS_2$) and 4 times (KDP)	12.8 × AGS (on powder)

Table 7.
Space group, band gap, transparency range, and SHG value of oxide crystal.

vfrom 1.2 to 40 mm. $BaMgF_4$ is a ferroelectric fluoride due to its wide transparency between 125 nm and 13 mm, and it can be used for UV and mid-IR optical applications [71, 72]. In the UV region, the shortest band is noted at 368 nm, which represents the potential behavior of $BaMgF_4$ as a nonlinear material. It can be used for the production of all solid-state lasers and mid-IR wavelength areas. $BaMgF_4$ and $SrAlF_5$ crystals are promising crystals for solid-state lasers. The LDT value of the $HgBr_2$ crystal is 0.3 GW/cm^2.

7. Oxyhalides

To develop high efficiency in mid-IR-NLO crystals, it is important to have an oxide-based system with an expandable IR transparent range. Many NLO oxides have a range from 3 to 5 μm atmospheric windows. When compared with the $AgGaS_2$ (13 μm), the oxide-based materials, such as $La_3SnGa_5O_{14}$ and $Pb_{17}O_8Cl_{18,}$ have wide IR

Figure 6.
Crystal of Tl_3PbBr_5.

Crystal	Space group	SHG ($AgGaS_2$)	LDT ($AgGaS_2$)
$Pb_{13}O_6Cl_4Br_{10}$	*Fmm*2	0.6	3.0
$Pb_{13}O_6Cl_7Br_7$	*Fmm*2	0.8	3.2
$Pb_{13}O_6Cl_9Br_5$	*Fmm*2	0.9	4.0

Table 8.
Space group and SHG value of oxyhalides.

transparency between 12 and 13.9 μm. In this lead oxyhalide, NLO crystal $Pb_{17}O_8Cl_{18}$ plays an outstanding overall property. To obtain high LDT, halide and oxide-based crystals with high bandgaps are used. Nowadays, the mixture of heavy metal lone pair cation, Pb^{2+}, and mixed oxyhalides are focused on IR applications. Xinglong Chen et al. discovered the lead mixed oxyhalides, such as $Pb_{13}O_6C_{l9}Br_5$, $Pb_{13}O_6C_{l7}Br_7$, and $Pb_{13}O_6C_{l4}Br_{10}$ [73], which have broad IR transparency up to 14 μm, high SHG behavior (0.6–0.9 × $AgGaS_2$) and wide bandgaps from 3.05 to 3.21 eV. $Pb_{13}O_6C_{l9}Br_5$ single crystal has the size of 2.9 × 1.3 × 0.5 cm^3, which was grown using the top-seeded solution growth (TSSG) method. It has a wide transparent range from 0.384 to 14.0 μm and a high LDT value (14.6 × $AgGaS_2$). Many crystals, such as $APbCO_3F$ (A = Rb, Cs), Pb_2BO_3Cl, $Cs_3VO(O_2)_2CO_3$, Bi_3TeBO_9, and $BiFSeO_3$ [74–78], have been reported with outstanding properties and it is a very good material for visible/near-IR nonlinear optical applications. $Pb_{13}O_6C_{l4}Br_{10}$, $Pb_{13}O_6C_{l7}Br_7$, and $Pb_{13}O_6C_{l9}Br_5$ have orthorhombic crystal structures with space group *Fmm*2 (**Table 8**). These three crystals are isomorphic.

By using Czochralski and flux method, oxide-based crystals can be obtained. The $Pb_{13}O_6C_{l4}Br_{10}$, $Pb_{13}O_6C_{l7}Br_7$, and $Pb_{13}O_6C_{l9}Br_5$ crystals were grown by flux method and the self-flux method was adopted for $PbCl_2$-$PbBr_2$. The crystals obtained by this method were optically transparent and they showed a good growth rate. $Pb_{13}O_6Cl_9Br_5$ was used to grow large-size crystals using the TSSG technique. After many technical optimizations, two big size crystals (Dimensions up to 2.9 × 1.3 × 0.5 and 3.7 × 0.4 × 0.7 cm^3) were grown using the [001] and [100] oriented seeds. They have good transparency and good growth speed. Therefore, to get a better quality crystal the growth parameters (cooling rate, rotation speed, and temperature gradient) are very important in the crystallization process. DSC curves of $Pb_{13}O_6Cl_4Br_{10}$, $Pb_{13}O_6Cl_7Br_7$, and $Pb_{13}O_6Cl_9Br_5$ show that each of them has one endothermic peak at 501°C, 504°C, and 508°C, respectively, which belongs to the melting point and these crystals have two exothermic peaks, which indicate the decomposing of the compounds. Due to the volatility of the halide materials, there is no weight loss before 490°C in the TGA curves. From the DSC and TGA, it was concluded that these compounds have high thermal stability up to 490°C. $Pb_{13}O_6C_{l9}Br_5$, $Pb_{13}O_6C_{l7}Br_7$, and $Pb_{13}O_6C_{l4}Br_{10}$ have high reflectance wavelengths in the region between 500 and 2500 nm. When compared

with $AgGaS_2$ (2.67 eV, 0.53–13 μm) and $ZnGeP_2$ (1.68 eV, 0.74–12 μm), the crystals of $Pb_{13}O_6C_{l4}Br_{10}$, $Pb_{13}O_6C_{l7}Br_{7,}$ and $Pb_{13}O_6C_{l9}Br_5$ own greater energy gaps and good transparency in IR region [79, 80].

In the application of high-power laser systems, the NLO crystal with laser-induced damage is one of the biggest problems. The crystals which have wider bandgaps are subjected to higher LDTs. Polycrystalline samples are used for the laser-induced damage threshold evaluation, and the polycrystalline material of $AgGaS_2$ was used as reference material. The $Pb_{13}O_6C_{l4}Br_{10}$, $Pb_{13}O_6C_{l7}Br_{7,}$ and $Pb_{13}O_6C_{l9}Br_5$ have large LDTs values, which are 3.0, 3.2, and 4.0 times higher than that of $AgGaS_2$. The $Pb_{13}O_6C_{l9}Br_5$ crystal has LDT of 439 MW/cm^{2,} this is 14.6 times higher than that of the $AgGaS_2$ crystal (30 MW/cm^2). The second harmonic generation intensity is 0.5 times higher than that of $AgGaS_2$. The SHG value of $Pb_{13}O_6C_{l4}Br_{10}$, $Pb_{13}O_6C_{l7}Br_{7,}$ and $Pb_{13}O_6C_{l9}Br_5$ are found to be 0.6, 0.8, and 0.9, respectively. From this, we concluded that SHG responses of each material have all phase-matchable when it is under the 2090 nm wavelength. Due to the increase in particle size, it showed a positive movement in SHG response.

8. Conclusion

In summary, significant progress has been attained in the search for new, favorable IR nonlinear crystals, such as chalcogenides, chalcohalides, oxides, halides, and oxyhalides, for producing coherent energy in the MIR. For a good NLO crystal, the crystals must have good physical and chemical properties, such as wide transparency range, LDT, chemical stability, birefringence, and nonlinear susceptibility. Nevertheless, for practical applications, the crystals should have high qualities with promising properties. For promising optical applications, accurate optical properties should be measured. For MIR applications, high bandgap value, LDT, and NLO susceptibility optical transparency are important. Various IR crystals fulfill the basic conditions of IR-NLO applications. The significant behavior of these crystals recommends that this crystal can be used in different optical applications.

Recent Advances in Infrared Nonlinear Optical Crystal
DOI: http://dx.doi.org/10.5772/intechopen.108173

Author details

Senthil Kumar Chandran[1*], Chinnakannu Elavarasi[2], Srinivasan Manikam[3] and Gnanapragasam John James[4]

1 Department of Physics, Government Arts and Science College, Hosur, Tamil Nadu, India

2 Sri Vijay Vidyalaya College of Arts and Science, Dharmapuri, Tamil Nadu, India

3 Department of Physics, Center for Crystal Growth, SSN College of Engineering, Kalavakkam, Tamil Nadu, India

4 Department of Physics, Government Arts College, Trichy, Tamil Nadu, India

*Address all correspondence to: senthilkumarchandran89@gmail.com

References

[1] Yan M, Xue HG, Guo SP. Recent achievements in lone-pair cation-based infrared second-order nonlinear optical materials. Crystal Growth & Design. 2020;**21**(1):698-720

[2] Chen X, Ok KM. Recent advances in oxide-based nonlinear optical materials with wide infrared transparency beyond 6 μm. Chemistry, an Asian Journal. 2020;**15**(22):3709-3716

[3] Liang F, Kang L, Lin Z, Wu Y. Mid-infrared nonlinear optical materials based on metal chalcogenides: Structure–property relationship. Crystal Growth & Design. 2017;**17**(4):2254-2289

[4] Gao L, Huang J, Guo S, Yang Z, Pan S. Structure-property survey and computer-assisted screening of mid-infrared nonlinear optical chalcohalides. Coordination Chemistry Reviews. 2020;**421**:213379

[5] Jiang XM, Guo SP, Zeng HY, Zhang MJ, Guo GC. Large crystal growth and new crystal exploration of mid-infrared second-order nonlinear optical materials. Structure-Property Relationships in Non-Linear Optical Crystals II. 2012;**2012**:1-43

[6] Isaenko LI, Yelisseyev AP. Recent studies of nonlinear chalcogenide crystals for the mid-IR. Semiconductor Science and Technology. 2016;**31**(12):123001

[7] Shi ZH, Chi Y, Sun ZD, Liu W, Guo SP. Sn2Ga2S5: A type of IR nonlinear-optical material. Inorganic Chemistry. 2019;**58**(18):12002

[8] Nguyen V, Ji B, Wu K, Zhang B, Wang J. Unprecedented mid-infrared nonlinear optical materials achieved by crystal structure engineering, a case study of (KX) P 2 S 6 (X= Sb, Bi, Ba). Chemical Science. 2022;**13**(9):2640-2648

[9] Wu C, Lin L, Jiang X, Lin Z, Huang Z, Humphrey MG, et al. K5 (W3O9F4) (IO3): An efficient mid-infrared nonlinear optical compound with high laser damage threshold. Chemistry of Materials. 2019;**31**(24):10100-10108

[10] Yu T, Wang S, Zhang X, Li C, Qiao J, Jia N, et al. MnSiP2: A new Mid-IR ternary phosphide with strong SHG effect and ultrabroad transparency range. Chemistry of Materials. 2019;**31**(6):2010-2018

[11] Guo SP, Chi Y, Guo GC. Recent achievements on middle and far-infrared second-order nonlinear optical materials. Coordination Chemistry Reviews. 2017;**335**:44-57

[12] Guo Y, Liang F, Yin W, Li Z, Luo X, Lin ZS, et al. BaHgGeSe4 and SrHgGeSe4: Two new Hg-based infrared nonlinear optical materials. Chemistry of Materials. 2019;**31**(8):3034-3040

[13] Li MY, Ma Z, Li B, Wu XT, Lin H, Zhu QL. HgCuPS4: An exceptional infrared nonlinear optical material with defect diamond-like structure. Chemistry of Materials. 2020;**32**(10):4331-4339

[14] Kushwaha AK, Kalita H, Suman S, Bhardwaj A, Ghosh R. Two-dimensional (2D) thermoelectric materials. Thermoelectricity and Advanced Thermoelectric Materials. 2021:233-260

[15] Muslih EY, Munir B, Khan MM. Advances in chalcogenides and chalcogenides-based nanomaterials such as sulfides, selenides, and tellurides. Chalcogenide-Based Nanomaterials as Photocatalysts. 2021:7-31

[16] Shi W, Ding YJ, Fernelius N, Vodopyanov K. Efficient, tunable, and coherent 0.18-5.27-THz source based on GaSe crystal. Optics Letters. 2002;**27**(16):1454-1456

[17] Abudurusuli A, Li J, Pan S. A review on the recently developed promising infrared nonlinear optical materials. Dalton Transactions. 2021;**50**(9):3155-3160

[18] Nitsche R, Bölsterli HU, Lichtensteiger M. Crystal growth by chemical transport reactions—I: Binary, ternary, and mixed-crystal chalcogenides. Journal of Physics and Chemistry of Solids. 1961;**21**:199-205

[19] Bajpai PK, Yadav S, Tiwari A, Virk HS. Recent advances in the synthesis and characterization of chalcogenide nanoparticles. Solid State Phenomena. 2015;**222**:187-233

[20] Jiang X, Kang L, Luo S, Gong P, Lee MH, Lin Z. Development of nonlinear optical materials promoted by density functional theory simulations. International Journal of Modern Physics B. 2014;**28**(27):1430018

[21] Ohmer MC, Goldstein JT, Zelmon DE, Saxler AW, Hegde SM, Wolf JD, et al. Infrared properties of AgGaTe 2, a nonlinear optical chalcopyrite semiconductor. Journal of Applied Physics. 1999;**86**(1):94-99

[22] Schunemann PG, Setzler SD, Pollak TM, Ohmer MC, Goldstein JT, Zelmon DE. Crystal growth and properties of AgGaTe2. Journal of Crystal Growth. 2000;**211**:242-246

[23] Isaenko L, Yelisseyev A, Lobanov S, Titov A, Petrov V, Zondy JJ, et al. Growth and properties of LiGaX2 (X= S, Se, Te) single crystals for nonlinear optical applications in the mid-IR. Crystal Research and Technology: Journal of Experimental and Industrial Crystallography. 2003;**38**:379-387

[24] Yelisseyev A, Isaenko L, Lovanov S, Zondy JJ. Advanced solid state lasers. OSA Trends in Optics and Photonics Series. 2000;**34**:561-569

[25] Zondy JJ, Bielsa F, Douillet A, Hilico L, Acef O, Petrov V, et al. Frequency doubling of CO 2 laser radiation at 10.6 μm in the highly nonlinear chalcopyrite LiGaTe 2. Optics Letters. 2007;**32**(12):1722-1724

[26] Yao J, Mei D, Bai L, Lin Z, Yin W, Fu P, et al. BaGa4Se7: A new congruent-melting IR nonlinear optical material. Inorganic Chemistry. 2010;**49**(20):9212-9216

[27] Yao J, Yin W, Feng K, Li X, Mei D, Lu Q, et al. Growth and characterization of BaGa4Se7 crystal. Journal of Crystal Growth. 2012;**346**(1):1-4

[28] Isaenko L, Yelisseyev A, Lobanov S, Krinitsin P, Petrov V, Zondy JJ. Ternary chalcogenides LiBC2 (B= In, Ga; C= S, Se, Te) for mid-IR nonlinear optics. Journal of Non-Crystalline Solids. 2006;**352**:2439-2443

[29] Yelisseyev AP, Drebushchak VA, Titov AS, Isaenko LI, Lobanov SI, Lyapunov KM, et al. Thermal properties of the mid-infrared nonlinear crystal LiInSe 2. Journal of Applied Physics. 2004;**96**(7):3659-3665

[30] Petrov V, Yelisseyev A, Isaenko L, Lobanov S, Titov A, Zondy JJ. Second-harmonic generation and optical parametric amplification in the mid-IR with orthorhombic biaxial crystals LiGaS2 and LiGaSe2. Applied Physics B. 2004;**78**(5):543-546

[31] Badikov V, Badikov D, Shevyrdyaeva G, Tyazhev A, Marchev G,

Panyutin V, et al. BaGa 4 S 7: Wide-bandgap phase-matchable nonlinear crystal for the mid-infrared. Optical Materials Express. 2011;**1**(3):316-320

[32] Tyazhev A, Kolker D, Marchev G, Badikov V, Badikov D, Shevyrdyaeva G, et al. Midinfrared optical parametric oscillator based on the wide-bandgap BaGa 4 S 7 nonlinear crystal. Optics Letters. 2012;**37**(19):4146-4148

[33] Medina-Ramírez I, Hernández-Ramírez A, Maya-Trevino ML. Synthesis methods for photocatalytic materials. In Photocatalytic Semiconductors. 2015:69-102

[34] Isaenko LI, Yelisseyev AP, Lobanov SI, Krinitsin PG, Molokeev MS. Structure and optical properties of Li2Ga2GeS6 nonlinear crystal. Optical Materials. 2015;**47**:413-419

[35] Yelisseyev AP, Isaenko LI, Krinitsin P, Liang F, Goloshumova AA, Naumov DY, et al. Crystal growth, structure, and optical properties of LiGaGe2Se6. Inorganic Chemistry. 2016;**55**(17):8672-8680

[36] Yin W, Feng K, Hao W, Yao J, Wu Y. Synthesis, structure, and properties of li2in2mq6 (m= si, ge; q= s, se): A new series of ir nonlinear optical materials. Inorganic Chemistry. 2012;**51**(10):5839-5843

[37] Lin X, Guo Y, Ye N. BaGa2GeX6 (X= S, Se): New mid-IR nonlinear optical crystals with large band gaps. Journal of Solid State Chemistry. 2012;**195**:172-177

[38] Liu PF, Li YY, Zheng YJ, Yu JS, Duan RH, Chen H, et al. Tailored synthesis of nonlinear optical quaternary chalcohalides: Ba 4 Ge 3 S 9 Cl 2, Ba 4 Si 3 Se 9 Cl 2 and Ba 4 Ge 3 Se 9 Cl 2. Dalton Transactions. 2017;**46**(8):2715-2721

[39] Feng K, Kang L, Lin Z, Yao J, Wu Y. Noncentrosymmetric chalcohalide NaBa 4 Ge 3 S 10 Cl with large bandgap and IR NLO response. Journal of Materials Chemistry C. 2014;**2**(23):4590-4596

[40] Liu BW, Zeng HY, Jiang XM, Wang GE, Li SF, Xu L, et al. [A 3 X] [Ga 3 PS 8] (A= K, Rb; X= Cl, Br): Promising IR non-linear optical materials exhibiting concurrently strong second-harmonic generation and high laser-induced damage thresholds. Chemical Science. 2016;**7**(9):6273-6277

[41] Guo SP, Sun ZD, Chi Y, Xue HG. Adduct-type IR nonlinear-optical crystal SbI3·(S8) 3 with a large second-harmonic generation and a high laser-induced damage threshold. Inorganic Chemistry. 2018;**57**(17):11282-11288

[42] Samoc A, Samoc M, Prasad PN, Krajewska-Cizio A. Second-harmonic generation in the crystalline complex antimony triiodide–sulfur. JOSA B. 1992;**9**(10):1819-1824

[43] Lu ZT, Sun ZD, Chi Y, Xue HG, Guo SP. Balanced second-order nonlinear optical properties of adducts CHI3·(S8) 3 and AsI3·(S8) 3: A systematic survey. Inorganic Chemistry. 2019;**58**(7):4619-4625

[44] Guo SP, Chi Y, Xue HG. SnI4·(S8) 2: A novel adduct-type infrared second-order nonlinear optical crystal. Angewandte Chemie. 2018;**130**(36):11714-11717

[45] Wiegers GT, Vos A. Refinement of the structure of tetrathiazylfluoride (NSF) 4. Acta Crystallographica. 1963;**16**(2):152-153

[46] Weiss J, Ruppert I, Appel R. Die Kristall-und Molekülstruktur von S3N5PF2. Zeitschrift für Anorganische

und Allgemeine Chemie. 1974;**406**:329-336

[47] Beck J, Schlueter S, Zotov N. The cube-shaped main group element clusters (Bi4S4)4+ and (Bi4Se4)4+- synthesis from chloroaluminate melts, crystal structures and vibrational spectra. Zeitschrift für Anorganische und Allgemeine Chemie. 2004;**630**:2512-2519

[48] Nickel V, Deiseroth HJ, Kienle L, Duppel V, Reiner C. Polymorphism of In5S5Cl–X-ray and HRTEM-Investigations. Allg. Chem. 2010;**636**:79-84

[49] Deiseroth HJ, Reiner C, Xhaxhiu K, Schlosser M, Kienle L. X-Ray and transmission electron microscopy investigations of the new solids In5S5Cl, In5Se5Cl, In5S5Br, and In5Se5Br. Zeitschrift für Anorganische und Allgemeine Chemie. 2004;**630**:2319-2328

[50] Wolmershäuser G, Krüger C, Tsay YH. [CS3N2Br]+ Br–ein Produkt der Bromierung von S4N4 in Schwefelkohlenstoff. Chemische Berichte. 1982;**115**(3):1126-1131

[51] Keller HL, Wimbert L. Über Münzmetall-Quecksilber-Chalkogenidhalogenide. III Zur Kristallstruktur von Ag2HgSI2. Zeitschrift für Anorganische und Allgemeine Chemie. 2003;**629**(12-13):2337-2340

[52] Biegerl A, Brunner E, Gröger C, Scheer M, Wachter J, Zabel M. The unexpected versatility of P4S3 as a building block in polymeric copper halide networks: 2, 3-P, 1, 2, 3-P and all-P coordination. Chemistry – A European Journal. 2007;**13**(33):9270-9276

[53] Zhang W, Tao X, Zhang C, Gao Z, Zhang Y, Yu W, et al. Bulk growth and characterization of a novel nonlinear optical crystal BaTeMo2O9. Crystal Growth & Design. 2008;**8**(1):304-307

[54] Jin CG, Li Z, Huang LX, He MZ. Top-seeded solution growth and characterization of a novel nonlinear optical crystal MnTeMoO6. Journal of Crystal Growth. 2013;**369**:43-46

[55] Zhang J, Tao X, Sun Y, Zhang Z, Zhang C, Gao Z, et al. Top-seeded solution growth, morphology, and properties of a polar crystal Cs2TeMo3O12. Crystal Growth & Design. 2011;**11**(5):1863-1868

[56] Zhang W, Wang X, Shen G, Shen D. Top-seeded growth, optical properties and theoretical studies of noncentrosymmetric Te2V2O9. Crystal Research and Technology. 2012;**47**:163-168

[57] Chen Z, Zhang Z, Dong X, Shi Y, Liu Y, Jing Q. Li3VO4: A promising mid-infrared nonlinear optical material with large laser damage threshold. Crystal Growth & Design. 2017;**17**:2792-2800

[58] Han G, Wang Y, Su X, Yang Z, Pan S. Growth, properties, and theoretical analysis of M2LiVO4 (M = Rb, Cs) crystals: Two potential mid-infrared nonlinear optical materials. Scientific Reports. 2017;**7**:1901

[59] Xu J, Wu H, Yu H, Zhang W, Hu Z, Wang J, et al. Li2K4TiOGe4O12: A stable mid-infrared nonlinear optical material. Chemistry of Materials. 2020;**32**:906-912

[60] Xi M, Tang C, Li R. Rb4Li2TiOGe4O12: A titanyl nonlinear optical material with the widest transparency range. Angewandte Chemie, International Edition. 2019;**58**:18257-18260

[61] Zhang H, Zhang M, Pan S, Dong X, Yang Z, Hou X, et al. Pb17O8Cl18: A

promising IR nonlinear optical material with large laser damage threshold synthesized in an open system. Journal of the American Chemical Society. 2015;**137**:8360-8363

[62] Lu W, Gao Z, Liu X, Tian X, Wu Q, Li C, et al. Rational design of a LiNbO3-like nonlinear optical crystal, Li2ZrTeO6, with high laser-damage threshold and wide Mid-IR transparency window. Journal of the American Chemical Society. 2018;**140**:13089-13096. DOI: 10.1021/jacs.8b08803

[63] Ok KM, Halasyamani PS, Casanova D, Llunell M, Alemany P, Alvarez S. Distortions in octahedrally coordinated d0 transition metal oxides: A continuous symmetry measures approach. Chemistry of Materials. 2006;**18**:3176-3183

[64] Lan H, Liang F, Jiang X, Zhang C, Yu H, Lin Z, et al. Pushing nonlinear optical oxides into the mid-infrared spectral region beyond 10 μm: Design, synthesis, and characterization of La3SnGa5O14. Journal of the American Chemical Society. 2018;**140**:4684-4690

[65] Hagemann M, Weber HJ. Are ternary halides useful materials for nonlinear optical applications? Applied Physics A. 1996;**63**(1):67-74

[66] Zhu T, Chen X, Qin J. Research progress on mid-IR nonlinear optical crystals with high laser damage threshold in China. Frontiers of Chemistry in China. 2011;**6**(1):1-8

[67] Singh NB, Suhre DR, Green K, Fernelius N, Hopkins FK. Periodically poled materials for long-wavelength infrared (LWIR) NLO applications. Journal of Crystal Growth. 2005;**274**:132-137

[68] Ferrier A, Velázquez M, Pérez O, Grebille D, Portier X, Moncorgé R. Crystal growth and characterization of the non-centrosymmetric compound Tl3PbCl5. Journal of Crystal Growth. 2006;**291**(2):375-384

[69] Ferrier A, Velázquez M, Portier X, Doualan JL, Moncorgé R. Tl3PbBr5: A possible crystal candidate for middle infrared nonlinear optics. Journal of Crystal Growth. 2006;**289**(1):357-365

[70] Badikov DV, Badikov VV, Kuz'micheva GM, Panyutin VL, Rybakov VB, Chizhikov VI, et al. Growth and X-ray diffraction study of Tl4HgI6 crystals. InorganicMaterials. 2004;**40**:314-320

[71] Shimamura K, Víllora EG, Muramatsu K, Ichinose N. Advantageous growth characteristics and properties of SrAlF5 compared with BaMgF4 for UV/VUV nonlinear optical applications. Journal of Crystal Growth. 2005;**275**:128-134

[72] Ravez J, Simon A, Chaminade JP. Ferroelectric behavior and phase transition at 715 K in $SrAlF_5$. Journal of Applied Physics. 1981;**52**:4740-4743

[73] Chen X, Jo H, Ok KM. Lead mixed oxyhalides satisfying all fundamental requirements for high-performance mid-infrared nonlinear optical materials. Angewandte Chemie. 2020;**132**(19):7584-7590

[74] Zou G, Lin C, Jo H, Nam G, You TS, Ok KM. Pb2BO3Cl: A Tailor-Made polar lead borate chloride with very strong second harmonic generation. Angewandte Chemie. 2016;**128**(39):12257-12261

[75] Zou G, Lin Z, Zeng H, Jo H, Lim SJ, You TS, et al. Cs 3 VO (O 2) 2 CO 3: An exceptionally thermostable carbonatoperoxovanadate with an extremely large second-harmonic

generation response. Chemical Science. 2018;**9**(48):8957-8961

[76] Xia M, Jiang X, Lin Z, Li R. "All-three-in-one": A new bismuth–tellurium–borate Bi3TeBO9 exhibiting strong second harmonic generation response. Journal of the American Chemical Society. 2016;**138**(43):14190-14193

[77] Zou G, Ye N, Huang L, Lin X. Alkaline-alkaline earth fluoride carbonate crystals ABCO3F (A= K, Rb, Cs; B= Ca, Sr, Ba) as nonlinear optical materials. Journal of the American Chemical Society. 2011;**133**(49):20001-20007

[78] Liang ML, Hu CL, Kong F, Mao JG. BiFSeO3: An excellent SHG material designed by aliovalent substitution. Journal of the American Chemical Society. 2016;**138**:9433-9436

[79] Kubelka P. Ein Beitrag zur Optik der Farbanstriche (Contribution to the optic of paint). Zeitschrift fur technische Physik. 1931;**12**:593-601

[80] Tauc J. Absorption edge and internal electric fields in amorphous semiconductors. Materials Research Bulletin. 1970;**5**(8):721-729